

# Landsat TM derived and in situ summer reflectance of glaciers in Svalbard

JAN-GUNNAR WINTHER



Winther, J-G. 1993: Landsat TM derived and in situ summer reflectance of glaciers in Svalbard. *Polar Research* 12(1), 37–55.

The paper presents satellite-derived and in situ reflectance from the Austre Brøggerbreen and Midre Lovénbreen glaciers located 78°50'N, 11°50'E in the Svalbard archipelago. The satellite data are Landsat-5 TM images recorded on 7 August 1987 and 31 August 1988. In situ measurements of shortwave and spectral reflectance of snow, glacier ice and moraine were carried out in August 1991 and in June 1992. In 1987, Austre Brøggerbreen had a positive net mass balance of +0.22 m of water equivalent while the net mass balance in 1988 was negative (–0.52 m). This is reflected in the atmospherically corrected satellite-derived albedo which shows that the reflective characteristics of the ablation and accumulation zones are more uniform and better separated in 1987 than in 1988. Besides the long-term year to year variations of surface albedo, the glaciers show a considerable short-term as well as spatial variability in reflectance. For example, the satellite-derived TM Band 4 albedo was found to vary between 0.19 and 0.65 at Midre Lovénbreen on 31 August 1988. In situ measurements show a drop in daily mean albedo from 0.88 to 0.13 during 4 days at a fixed location on Austre Brøggerbreen in August 1991 (300 m.a.s.l.). Furthermore, spectral measurements of snow albedo in June 1992 clearly demonstrate that the near-infra-red albedo decreases when the snow metamorphoses, i.e. when the characteristic grain size increases. The effect of cloud cover on the snow albedo is also discussed. The integrated albedo (370–900 nm) increased from 0.812 to 0.869 (7%) when the weather condition changed from clear sky to 100% overcast within 2 hours on 9 June 1992. The bidirectional reflectance of snow is measured by taking spectral scans for viewing angles 0° (nadir), 15°, 30°, 45° and 60° for viewing directions facing the sun and at azimuths 90° and 180° away from the sun. The increase in albedo relative to the nadir albedo is found to be 8, 15, 19 and 26% for viewing angles 15°, 30°, 45° and 60°, respectively. The largest anisotropy is seen for metamorphosed snow in measurements facing the sun. Consequently, it may be necessary to correct for the specular properties of snow if satellite-derived surface reflectance is going to be considered in terms of *absolute* values.

Jan-Gunnar Winther, SINTEF Norwegian Hydrotechnical Laboratory, N-7034 Trondheim, Norway.

## Introduction

Studies of the mass balance of the small glaciers of the world have become increasingly important as these glaciers respond to changes in regional climate on the scale of decades and can thus serve as indicators of regional climate change. Landsat multispectral scanner (MSS) and Landsat thematic mapper (TM) data have been available since 1972 and 1982, respectively. The satellite data provide digital images for analysing the position of the equilibrium line (Østrem 1975; Hall & Ormsby 1983), glacier facies (Williams et al. 1991), glacier reflectance (Zeng et al. 1984; Hall et al. 1987, 1989, 1990), terminus position and changes in glacier area (Hall et al. 1992a).

The ablation and accumulation areas of a glacier are separated by the equilibrium line. The

snow line is defined as the lower border of the snow from last winter and often represents the approximate location of the equilibrium line at the end of an average mass balance year. The equilibrium line altitude (ELA) can be well correlated with the net balance (Schytt 1981; Young 1981; Hagen & Liestøl 1990). Moreover, the digital Landsat TM data (30 metres pixel resolution) is well suited for positioning the snow line and thus can be used for studies of glacier mass balance. However, as a zone of superimposed ice can form between the snow line and the equilibrium line, the exact location of the equilibrium line can become complicated. Superimposed ice forms when water percolates through the wet snow and refreezes on the underlying glacier ice (Wakahama et al. 1976; Paterson 1981). A broad zone (up to 1 km) of superimposed ice is normally

formed at Austre Brøggerbreen, making the positioning of the equilibrium line by satellite remote sensing difficult.

The ablation area consists of exposed ice during the summer and represents an area where net loss occurs by melting. The accumulation area can be divided into the wet-snow, percolation and dry-snow facies. Obviously, the different facies represent snow and ice surfaces with quite different characteristics with respect to reflectance. Thus, the facies and their characteristic surface reflectance (or albedo) are important in terms of energy exchange between the glacier and the surrounding air mass. Even small changes in snow reflectance can have a significant effect on the Earth-atmosphere energy balance (Warren & Wiscombe 1985).

This paper mainly emphasises (1) temporal and spatial variations of glacier summer albedo, and (2) anisotropic snow reflectance and its effect on the calculated satellite-derived albedo. The study presents the satellite-derived glacier albedo recorded by Landsat-5 TM in August 1987 and August 1988 together with in situ albedo measurements of snow, ice and moraine in the same area in August 1991 and June 1992. Both the in situ and the satellite-derived measurements demonstrate the large range of surface albedo present on the glacier, especially at the end of the mass-balance year (i.e. normally in late August). Further, off-nadir spectral measurements of snow reflectance are presented and illustrate the anisotropic reflectance properties of snow. It is shown how the bidirectional reflectance of snow varies when the direction of the sensor changes both horizontally and vertically. The study points out that correction for anisotropic snow reflectance may be needed if the calculated satellite-derived snow albedos are going to be considered as *absolute* values.

## Study area

The Svalbard archipelago is situated between latitudes 76°N and 81°N and longitudes 10°E and 35°E in the Norwegian Arctic (Fig. 1). The total area is about 63,000 km<sup>2</sup> and 60% is covered by glaciers (Sand et al. 1991). The ice-free areas in Svalbard have continuous permafrost. The thickness of the permafrost varies from less than 100 m close to sea level up to 500 m in the higher mountainous areas (Liestøl 1977).

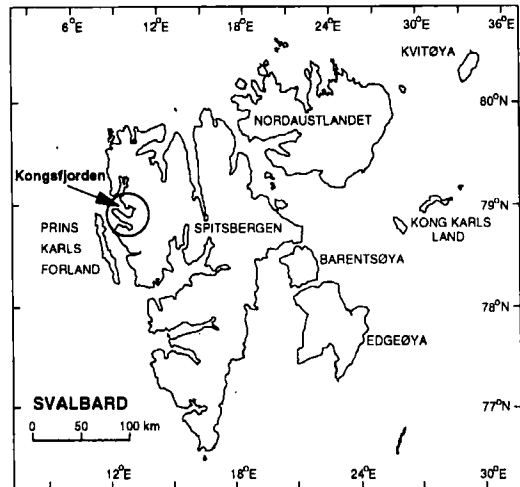


Fig. 1. The Svalbard archipelago and the study area (encircled).

The study area lies in the Kongsfjorden area on the western coast of Spitsbergen (Fig. 1). Several glaciers drain into the Kongsfjorden inlet and satellite-derived surface reflectance has been recorded for two of the glaciers, Austre Brøggerbreen and Midre Lovénbreen. In situ measurements were carried out on Austre Brøggerbreen in August 1991 and June 1992. Austre Brøggerbreen is the eastern part of the larger Brøggerbreen glacier (Figs. 2 and 3). Brøggerbreen glacier is a 5 km<sup>2</sup> subpolar glacier located 78°50'N, 11°50'E on the Brøggerhalvøya peninsula, close to the research station in Ny-Ålesund (Hagen et al. 1991). The glacier stretches from about 75 m.a.s.l. at its retreating front to about 575 m.a.s.l. The glacier front is flat and the main flow direction is towards the north. There are few crevasses on the glacier due to very slow movement of the ice mass. Mass balance measurements show a steadily decreasing ice mass since 1968 (Hagen & Liestøl 1990).

## Background and methods

### Glacier facies

Glaciers are composed of an ablation and an accumulation area. Within these two areas several facies might be present (Fig. 4). The facies represent distinctive areas with characteristics that

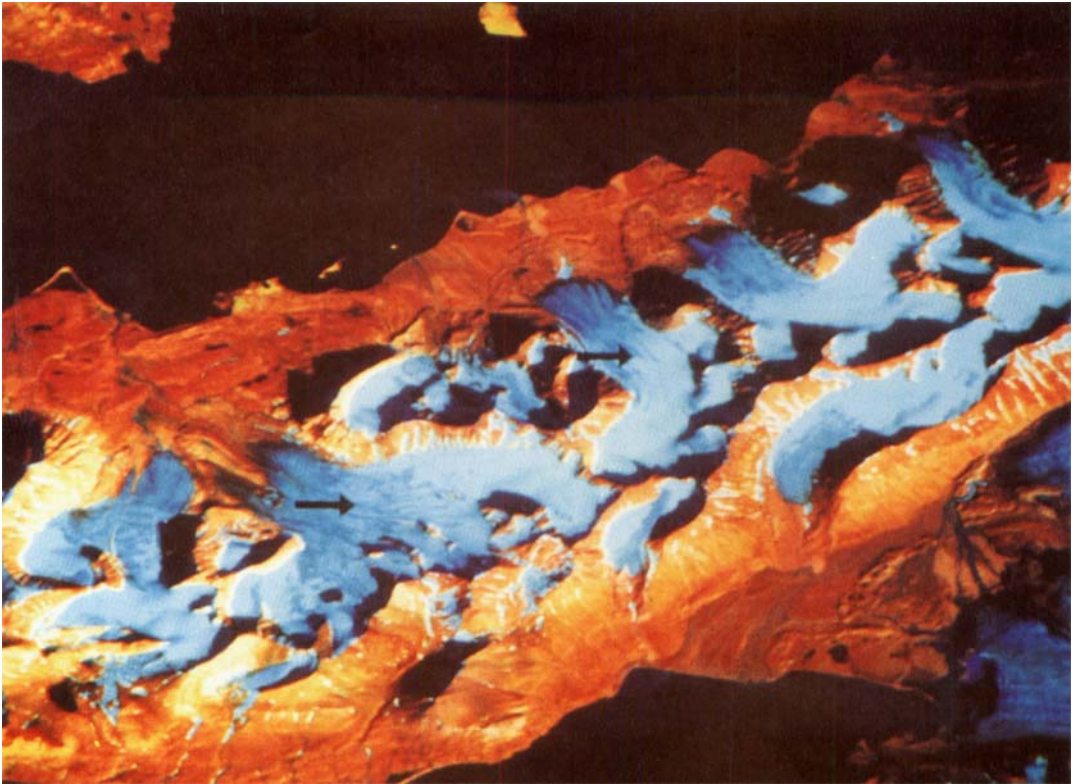


*Fig. 2.* Part of a Landsat Thematic Mapper TM Bands 2, 4 and 5 composite image recorded on 7 August 1987 (512 × 512 pixels). Austre Brøggerbreen (left arrow) and Midre Lovénbreen (right arrow) lie on the Brøggerhalvøya peninsula due south of the Kongsfjorden inlet. Austre Brøggerbreen terminates on land at about 75 m.a.s.l. The upper part of the glacier stretches up to 575 m.a.s.l. and the main flow direction is towards north i.e., towards the upper left corner of the image. The lower part of the glacier has low reflectance due to morainal deposits and exposed blue ice. A transition zone of superimposed ice is seen close to the arrow while the upper part is covered by snow.

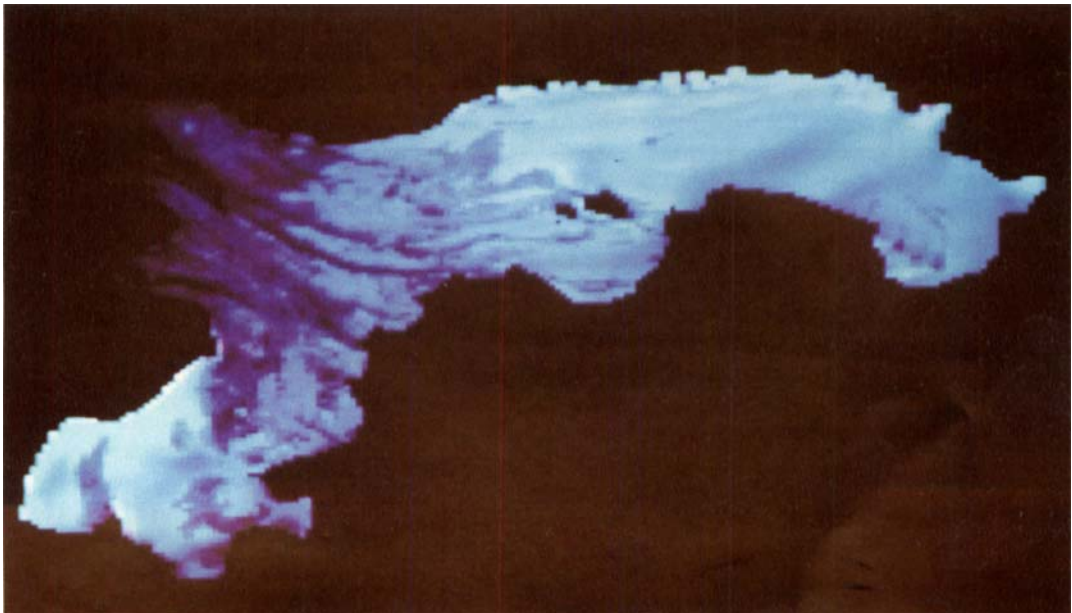


*Fig. 3.* Landsat Thematic Mapper TM Bands 2, 4 and 5 composite image of Austre Brøggerbreen recorded on 7 August 1987. Shaded areas of the glacier are masked out. Blue ice is exposed in the lower parts of the glacier (upper left). The superimposed ice zone can be seen left of the centre of the image (light blue) while the upper parts of the glacier constitute the wet-snow zone (right part of the image).

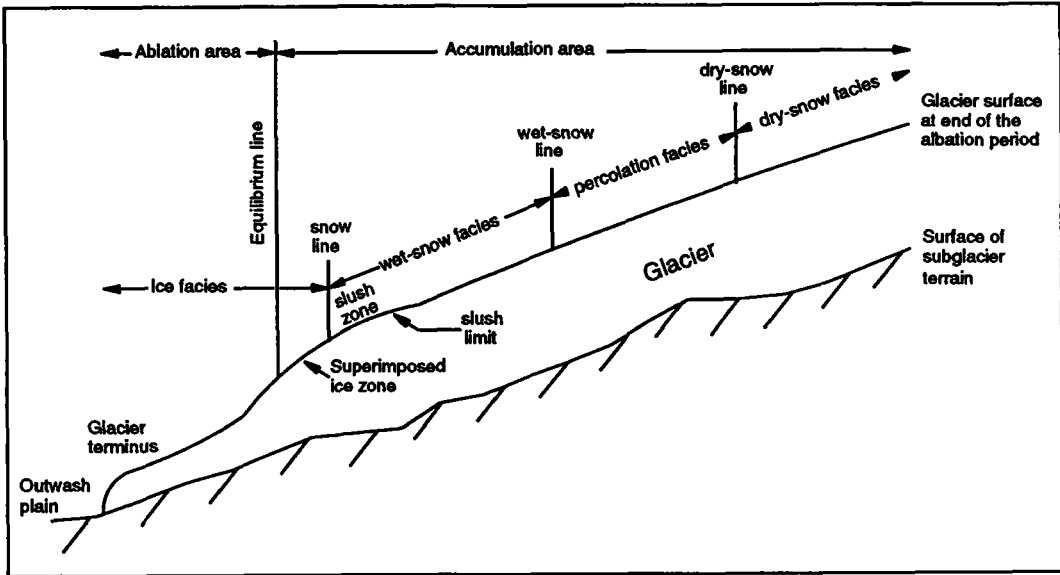


Fig. 4. Cross-section of a glacier showing facies at the end of the balance year from glaciological field observations (figure modified from Williams et al. 1991).

reflect the environment under which the snow or ice was formed. The accumulation area is typically composed of wet-snow facies, percolation facies and dry-snow facies (Benson 1959, 1967; Müller 1962; Benson & Motyka 1979; Williams et al. 1991). However, due to long periods of mild weather which influence the glacier surface at all altitude levels, the accumulation area of Austre Brøggerbreen consists predominantly of wet-snow facies at the end of the ablation period.

Superimposed ice is formed by (1) the refreezing of meltwater during the autumn and/or during the ablation period and (2) the refreezing of meltwater on the glacier surface below the snow line at the end of the ablation period (Parrot et al. 1993). Furthermore, net loss by melting occurs in the ice facies. On Austre Brøggerbreen the ice facies mainly consist of blue ice partly covered by morainal deposit. Consequently, the surface is honeycombed due to a non-uniform distribution of ablation. In addition, meltwater flow creates a complex surface pattern which looks like a grid system with irregular angles and highly varying dimensions in the x, y and z-directions. Because of the low reflectance, the ice facies can normally be easily distinguished from the snow facies. Even so, many natural features on a glacier can obscure

facies boundaries and make them hard to separate by satellite remote sensing. Such features can be a new snowfall or desert/volcanic dust (Hall et al. 1987). However, difficulties in separating the ablation area from the surrounding ice-free area are more common. This is because the low reflectance of the glacier terminus caused by rock debris, may be similar to the adjacent morainal and outwash-plain materials (Williams et al. 1991).

The equilibrium line altitude (ELA) often corresponds quite closely with the snow line altitude (Williams et al. 1991). However, Parrot et al. (1993) carried out a study on Austre Brøggerbreen and Midre Lovénbreen and pointed out that the ELA is located within the zone of superimposed ice on these glaciers. This is confirmed by Hagen & Liestøl (1990) who report that the altitude of the transient snow line may be far above the actual ELA, and the altitude difference varies just as the amount of superimposed ice varies. Today the ELA is located from stake readings on Austre Brøggerbreen. Hagen & Liestøl (1990) made use of simple linear regression analysis and calculated the correlation between the net mass balance and the ELA (1967–88) to be 0.961 and 0.953 for Austre Brøggerbreen and

Midre Lovénbreen, respectively. Thus, on glaciers where the ELA can be localized by satellite remote sensing techniques, this can give valuable information about the mass balance of these glaciers.

*Spectral reflectance of snow and glacier ice*

The portion of radiation reflected from a surface consisting of fresh snow remains high in the visible region while a distinct drop occurs in the near-infra-red (Fig. 5). Furthermore, the snow albedo drops below 0.10 in the middle-infra-red region where TM Bands 5 and 7 are located (outside the wavelength range shown in Fig. 5). TM Bands 1, 2 and 3 are sensitive to visible blackening of the snow surface such as deposition of dust and organic material (Dozier et al. 1981). Albedo reduction caused by snow grain coarsening and increasing liquid water content is most prominent in the near-infra-red making TM Band 4 the most appropriate band for detection of snow metamorphosis process (Bryazgin & Koptev 1969; Choudhury & Chang 1979).

Fig. 5. shows the spectral curves of fresh snow, firn, glacier ice, refreezing ice and dirty glacier ice. The visible reflectance declines from 0.95 to 0.60 as the snow cover metamorphoses to glacier ice (Fig. 5). A similar reduction of reflectance

takes place in the infra-red region. Consequently, all TM Bands 1–4 can be used to distinguish snow from firn and ice facies. Further downstream, the surface at the glacier terminus is honeycombed because of the dirty moraine and non-uniform distribution of ablation. The reflectance lies close to 0.6 for glacier ice and at about 0.2 for dirty glacier ice in the visible range, but increases a little in the infra-red due to the presence of moraine (Zeng et al. 1984). Thus, the visible TM Bands are suitable for separating dirty glacier ice from (clean) glacier ice whereas TM Band 4 is unsuited to this purpose. Finally, Fig. 5 shows that glacier ice has a larger reflectance than refreezing ice in the visible region while the opposite is the case in the infra-red region.

*The Landsat Thematic Mapper data set*

The Landsat-5 satellite, launched in March 1984, carries a Multispectral Scanner Subsystem (MSS) and a Thematic Mapper (TM) onboard. The TM senses in the following bands (Lillesand & Kiefer 1987):

TM1	0.45–0.52 $\mu\text{m}$
TM2	0.52–0.60 $\mu\text{m}$
TM3	0.63–0.69 $\mu\text{m}$
TM4	0.76–0.90 $\mu\text{m}$
TM5	1.55–1.75 $\mu\text{m}$
TM6	10.40–12.50 $\mu\text{m}$
TM7	2.08–2.35 $\mu\text{m}$

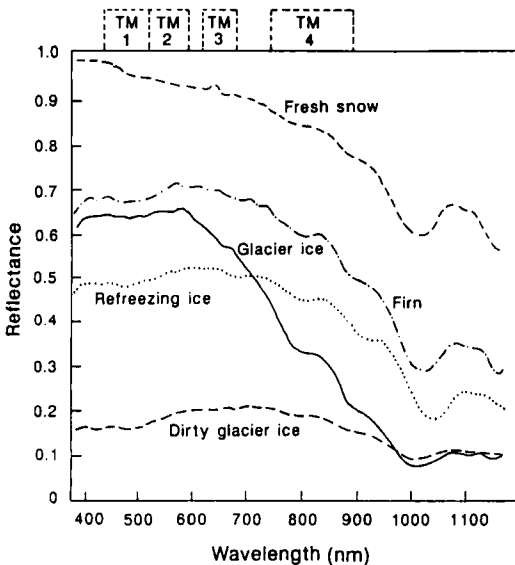


Fig. 5. Spectral reflectance curves for snow and ice in different formation stages (figure modified from Zeng et al. 1984).

TM Band 6 lies in the thermal-infra-red part of the EM spectrum and has a spatial resolution of 120 m. The other TM Bands (Bands 1–5 and 7) are located within the visible, near-infra-red and mid-infra-red wavelength regions. They have a spatial resolution of 30 m. Spectral signatures from snow at these wavelengths make them suitable for studies of grain size and surface impurities (Dozier 1984).

The images used in this study are Landsat-5 TM scenes from August 7, 1987, and August 31, 1988. Both images are cloud-free and are recorded at 12:21 and 11:44 (GMT), respectively. The solar elevation is 26.8° in the image from 1987 and 18.6° in the image from 1988. Data saturation is common in regions with high reflection such as snow-covered terrain and is reported by many investigators (Dozier 1985; Orheim & Lucchitta 1988; Hall et al. 1990). Severe data saturation occurs in TM Band 1 in both images.

By converting the digital numbers (DNs) obtained from the digital TM data, surface reflectance and thus the albedo was computed. A conversion procedure is described by Markham & Barker (1986). This method is widely used (Hall et al. 1988; Orheim & Lucchitta 1988; Dozier 1989) and is applied to the Landsat TM images used in this study as well. The conversion is important since albedo is a physical parameter and is used for example in General Circulation Models (GCMs) and in Energy Budget Models. The albedo is expressed as the ratio of total reflected radiation to total incident radiation. Total reflected radiation includes hemispherical surface reflection integrated over the reflective regions of the EM spectrum.

*Effects of atmosphere, topography and anisotropic reflectance on satellite-derived albedo*

Three important factors influence the accuracy of the calculated at-satellite planetary reflectance: (1) atmospheric effects caused by gaseous absorption and scattering by molecules and aerosols, (2) topographic effects due to the fact that illumination and reflectance from sloping areas deviate from the true spectral response characteristics to these areas, and (3) anisotropic snow reflectance because an increased portion of the scattering occurs in the forward direction as snow metamorphoses.

Atmospheric correction of the images is carried out using the 5S computer code for the simulation of satellite signals in the solar spectrum (Tanré et al. 1990). The 5S code allows the estimation of solar radiation backscattered by the Earth-surface-atmosphere system, as it is observed by a satellite sensor. Corrections are based on input specifications like geometrical conditions, atmospheric model (subarctic summer), aerosol characteristics (type and concentration), spectral band of observation and a given ground reflectance. For a specified ground reflectance the corresponding at-satellite reflectance is computed by the model. Then, apparent reflectance might be calculated for different specific ground reflectances, for example with increments of 0.1. Furthermore, simple linear regression using at-satellite reflectances as the independent variable and ground reflectance as the dependent variable has been carried out. When the regression equations are established, the ground reflectance

can easily be calculated for every pixel in the image. For the two TM images, the satellite-derived surface reflectance is underestimated if no correction is carried out.

Influence from topography can be separated in effects related to the illuminated pixel itself and to effects from adjacent slopes (Hall et al. 1988). With respect to the former, the geometry between the sun, the target orientation and the sensor might vary from one pixel to another. Therefore, this normally results in darker parts of the image facing away from the sun and the brighter areas being sun-facing slopes. The topographic effects are most pronounced at low solar elevations and for slopes close to the principal plane of the sun (Holben & Justice 1979). Concerning the latter, the topographic environment may (1) cast shadows on a pixel so that it receives no direct radiation at all, (2) reduce the scattered sky radiation by hiding a part of the sky hemisphere and (3) reflect the radiation towards the pixel, consequently giving an additional irradiance (Proy et al. 1989). Digital Terrain Models for topographic correction of the TM-images have not been used in this study. However, areas in shadow and areas where rocks stick out frequently (below and right of the arrow in Fig. 2) have been masked and excluded in the data presented in the Results and discussion section.

Snow is an anisotropic reflector after it has begun to metamorphose (Dirmhirn & Eaton 1975; Steffen 1987; Dozier et al. 1988; Hall et al. 1988, 1992b). Though freshly fallen snow can be considered a Lambertian reflector, as snow metamorphoses the specular component characteristic of forward scattering increases. Then, since the Landsat sensors are nadir-viewing, the satellite-derived reflectance will often provide different reflectances compared to the hemispherical reflectance on the ground. This subject is covered in more detail in the Results and discussion section.

*In situ instrumentation and measurements*

A Kipp and Zonen albedometer (model CM 7) measured the surface albedo on Austre Brøggerbreen at 300 m.a.s.l. from 16–28 August 1991. The albedometer consists of two identical pyranometers, model CM 5. One measures the incident solar radiation, the other the radiation reflected by the surface. When the output of the

pyranometers is recorded separately, the albedo can be calculated from the ratio between these outputs. White lacquered screens prevent the CM 7 albedometer housing from being heated by radiation. In addition, the lower screen prevents the illumination of the lower glass domes directly by the sun near sunrise and sunset. The albedometer is sensitive (panchromatic) for wavelengths from 305 nm to approximately 2800 nm. The logging interval was set to 10 minutes.

Initially, the sensor height was 1.55 m but increased to 1.85 m due to snow melting during the first week. Then, a storm broke out and the albedometer was lowered to 1.10 m to reduce the wind forces on the instrument and its stand. The illuminated surface consisted initially of 30 cm of wet snow with a characteristic grain size of 2–3 mm overlying the glacier ice. Gradually, the snow melted and the surface conditions turned to a mixture of snow, water puddles and blue ice. Later, a smooth slippery and wet blue ice surface was exposed. Finally, on the last day of measurements, fresh snow began to accumulate on the blue ice. In addition to the albedo recordings, air and snow temperature, density, liquid water content, grain size and shape, snow hardness and stratification were measured in shallow snow pits at height intervals of 25 m between 300 and 600 m.a.s.l. Grain size was registered by macro photography of snow grains placed on a black crystal screen with a white grid scale indicator. The snow pits were placed along the centre line of the glacier.

In 1992, in situ measurements were acquired using the SE 590 spectrometer. The SE 590 measures radiation between 370 and 1110 nm in 252 discrete steps, i.e. each channel represents a bandwidth of approximately 3 nm. The spectral resolution is about 10 nm. The field of view of the sensor is 6° and the surface area covered by the sensor represents about 14 cm<sup>2</sup> for the measurements presented here. The spectral detector head was fastened to a standard camera tripod to avoid movements during the integration time of the sensor that was less than 1 second. Immediately after each snow measurement sequence, a spectral measurement of a halon target at 0° nadir angle was taken as a reference for the calculations of albedo. The solar and atmospheric conditions are considered to be stable during one scan sequence. The limits of the sensitivity of the silicon detectors are reached in the near-infra-red region, and the signal-to-noise ratio is small

beyond 900 nm (Dozier et al. 1988; Hall et al. 1992b). Therefore, only data between 370 and 900 nm is presented. In addition to measurements of snow reflectance, some spectral reflectance curves of moraines in the terminus area were taken.

Daily measurements from 2–10 June 1992, of spectral reflectance of snow, air and snow temperature, density, liquid water content, grain size and shape, snow hardness and stratification were acquired at a measuring site downstream from the terminus of Austre Brøggerbreen at 15 m.a.s.l. These measurements were also carried out at height intervals of 25 m between 50 and 525 m.a.s.l. along the centre line of the glacier.

Scan sequences of snow reflectance were acquired by pointing the spectral detector head at nadir (0°), and 15°, 30°, 45° and 60° off-nadir followed by a nadir reference measurement of the halon target. Such a scan sequence typically took less than 2 min. The azimuthal directions of the measurements were towards the sun, and 90° and 180° away from the sun (Fig. 6). Shadows from the tripod introduced an error at some of the viewing angles under clear sky conditions for the measurements facing 180° away from the sun.

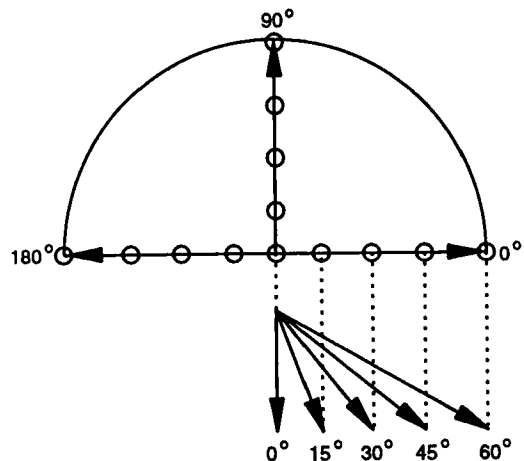


Fig. 6. Viewing geometry of the measurements. The upper part of the figure shows the horizontal viewing directions where 0° refers to measurements facing the sun. The lower part of the figure shows the vertical viewing directions for measurements facing the sun. Similar off-nadir measurements were made in the directions facing 90° and 180° away from the sun, i.e., each indicated point in the upper figure represents one spectral measurement.

## Results and discussion

### *Satellite-derived surface albedo of Austre Brøggerbreen and Midre Lovénbreen*

Both Austre Brøggerbreen and Midre Lovénbreen are masked out of the sub-image seen in Fig. 2. Fig. 3 shows Austre Brøggerbreen after the masking. Next, analysis of the two glaciers are made. Surface reflectance expressed by the DNs shows that the visible and near-infra-red reflectance (i.e. TM Bands 2 and 4) is generally higher in 1987 than in 1988 (Table 1). Only two years of positive net mass balance are recorded on Austre Brøggerbreen in the period 1966–1991 and the largest positive value is found in 1987 (+0.22 m of water equivalent). 1988 is close to a normal year with a net mass balance of  $-0.52$  m. The average net mass balance for 1966–91 is  $-0.42$  m (Hagen, pers. commun.).

Fig. 7 presents histograms showing the frequency of occurrence of each DN for TM Bands 2, 4 and 5 of Austre Brøggerbreen for 1987 and 1988. The TM Band 2 and TM Band 4 histograms for 1987 display two distinct peaks which reflect the different surface reflectance of the ablation and accumulation zones of the glacier. The shape of the two histograms is similar, although the TM Band 4 histogram is shifted towards smaller DNs. This indicates that the near-infra-red reflectance (TM Band 4) is lower than the visible reflectance (TM Band 2). In 1988, however, the peaks are not as pronounced because the transition from the ablation zone to the accumulation zone is indistinct. Areas of low reflectance are present within the accumulation zone and the ELA is located 440 m.a.s.l. at the end of the mass balance year in 1988 (Hagen, pers. commun.). Interestingly, a marked cleft is also present in the 1988 histograms in such a way that some of the DNs

are almost absent, especially in TM Band 4. This cleft probably represents the division between snow and blue ice. If so, the histograms confirm the situation present in these two years: (1) less blue ice is exposed in 1987 than in 1988 (the left peak is smaller in the 1987 histograms) and (2) the ablation and accumulation zones show less variability in the frequency of occurrence of the DNs and are better separated in 1987 (more distinct peaks with a larger interval in the 1987 histograms). The TM Band 5 histograms display low DNs for both years due to the very low reflectance of snow and ice at these wavelengths.

Austre Brøggerbreen and Midre Lovénbreen are divided into five height zones: 50–100 m, 100–200 m, 200–300 m, 300–400 m and >400 m, respectively. Variations in the surface reflectance as a function of altitude can be seen in Table 2 and are displayed in Fig. 8. The surface reflectance increases steadily as the altitude increases, except for the uppermost height zone of Austre Brøggerbreen (Fig. 8). Above about 400 m some areas of the glacier flatten out, delaying the downwards drainage of meltwater. Consequently, the meltwater which percolates through the snow pack and down to the surface of the glacier flows at a slow rate due to the gentle gradient. In some areas the meltwater drainage is hindered to such a degree that meltwater rises in the snow pack and even wets the surface. Spots with low surface reflectance are therefore common in this height zone.

Satellite-derived surface albedo is shown in Tables 3, 4, 5 and 6. As mentioned earlier, the calculation of albedo follows the procedure reported by Markham & Barker (1986) and Tanré et al. (1990). Topographic effects are only considered by removing shaded areas. Snow is regarded as an isotropic reflector.

### *In situ measurements of the albedo of snow, ice and moraine*

Fig. 9 shows the daily mean albedo (305 nm–2800 nm) measured at Austre Brøggerbreen at 300 m.a.s.l. from 16–28 August 1991. Fig. 10 displays the shortwave albedo variations on four selected days. Initially, e.g. on 16 August, the surface consisted of 30 cm wet snow with a grain size of 2–3 mm overlaying the glacier ice. Gradually the snow melted and the surface characteristics turned to a mixture of snow, water puddles and blue ice. This resulted in a pro-

*Table 1.* Statistics for TM bands 2, 4 and 5 of Austre Brøggerbreen. Landsat TM images were acquired on 7 August 1987 and 31 August 1988

	TM2		TM4		TM5	
	1987	1988	1987	1988	1987	1988
Mean (DN)	98.22	54.43	76.62	46.58	7.00	13.72
Maximum	147	97	135	98	66	29
Minimum	26	31	18	22	2	4
Std. Dev.	25.51	12.72	26.05	14.63	5.48	4.95

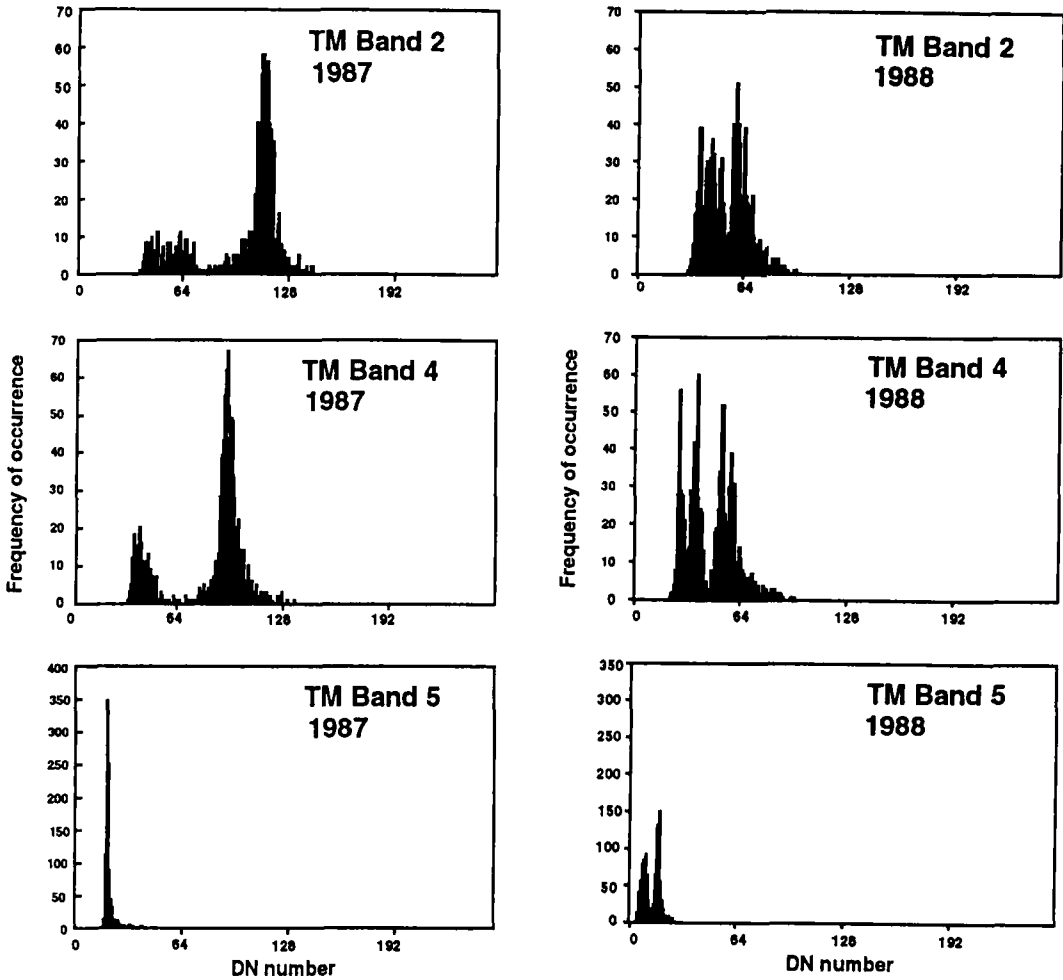


Fig. 7. Histograms showing the frequency of occurrence of each DN for TM Bands 2, 4 and 5 of Austre Brøggerbreen. Landsat TM images were acquired on 7 August 1987 and on 31 August 1988.

nounced drop in the surface albedo (Fig. 9). On 24 August a smooth, slippery and wet blue ice surface was exposed. Finally, fresh snow began

to accumulate on the blue ice and the albedo increased again. Fig. 9 clearly demonstrates how variable the albedo of the glacier can be during

Table 2. TM Band 4 statistics for five height zones of Austre Brøggerbreen: 50–100 m, 100–200 m, 200–300 m, 300–400 m and >400 m, respectively. The Landsat TM image was recorded on 7 August 1987.

	Zone I (50–100 m)	Zone II (100–200 m)	Zone III (200–300 m)	Zone IV (300–400 m)	Zone V (>400 m)
Mean (DN)	25.98	42.85	68.19	80.80	78.32
Maximum	54	77	132	167	115
Minimum	18	21	29	27	29
Std. Dev.	5.00	11.28	17.93	18.35	10.16
No. of pixels	253	1968	2938	1829	890

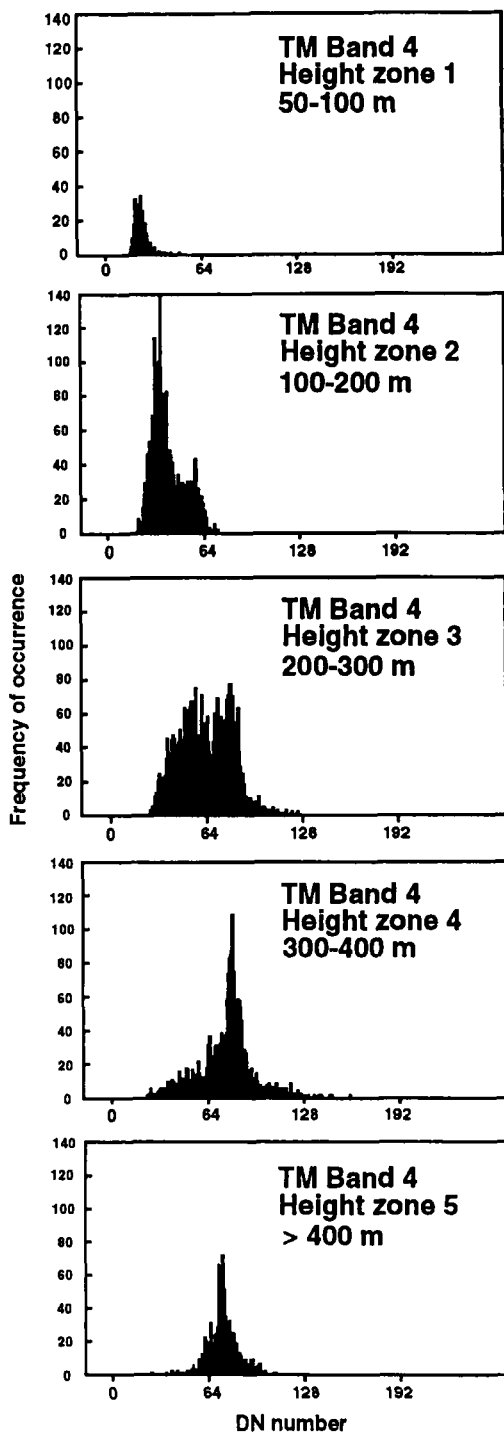


Fig. 8. Histograms displaying the frequency of occurrence of each DN for TM Band 4 for five different height zones on Austre Brøggerbreen: 50–100 m, 100–200 m, 200–300 m, 300–400 m and >400 m, respectively. The Landsat TM image was recorded on 7 August 1987.

this time of year when both intensive snow melt and accumulation of fresh snow can occur.

Visible and near-infra-red spectral albedo measurements of clean snow (fresh snow as well as metamorphosed snow) and moraines were acquired in June 1992 using the portable SE 590 spectrometer (Fig. 11). The top of the snow pack consisted of about 4 cm of fresh-fallen snow on 2 June. Underneath, the snow pack was composed of different layers of coarser snow which had previously undergone recrystallization (Table 7). The fresh snow causes the high albedo seen in Curve A (Fig. 11). The albedo of snow is 0.988 at 372 nm and remains larger than 0.95 up to 645 nm. Here, the albedo reduction becomes more prominent and the snow albedo becomes 0.856 at 900 nm. The average snow albedo between 372 and 900 nm is 0.941.

Curves B and C are from 9 June, after a week of on-going metamorphism in the snow pack. Air temperatures were both below and above zero in this period causing slow and irregular melting. The surface snow grains grew and were rounded, and the characteristic grain size increased from less than 1 mm on 2 June to 2–3 mm on 9 June (Table 7). On 9 June, the liquid water content was close to zero due to night-time freezing, creating a strong crust layer comprising the upper 9 cm of the snow cover. Curve B is taken at 15:30 (local summer time) at the same site as Curve A and under similar weather conditions (100% overcast) with mainly diffuse incoming radiation. Curve B displays a general decrease in albedo compared to Curve A (Fig. 11). Moreover, the decrease is more pronounced in the near-infra-red region where the albedo drops off quickly. Visible surface impurities were not seen on either 2 June or 9 June, and the albedo reduction is most probably caused by the increase in the snow grain size.

Curve C is taken under clear sky conditions at 13:30 (local summer time), two hours prior to Curve B. There were no noticeable changes in the snow surface characteristics during the two hour period. Two effects besides cloud conditions and instrumental errors might have contributed to a change in albedo: (1) the varying contribution of specular reflection from the snow surface with solar angle and (2) the metamorphism (recrystallization on the surface and within the snow pack). Regarding (1), the snow albedo increases as the solar elevation decreases because the first scattering event happens closer to the surface at low sun angles than at larger ones (Dirnhirn &

Table 3. Satellite-derived surface albedo for five height zones on Austre Brøggerbreen recorded on 7 August 1987<sup>a</sup>.

Height zone <sup>b</sup>	TM Band					
	1	2	3	4	5	7
I: 50–100 m	0.15 ± 0.04 <sup>c</sup>	0.17 ± 0.04	0.16 ± 0.03	0.14 ± 0.03	0.01 ± 0.00	0.01 ± 0.00
II: 100–200 m	0.26 ± 0.06	0.29 ± 0.06	0.27 ± 0.05	0.24 ± 0.06	0.01 ± 0.00	0.01 ± 0.00
III: 200–300 m	d	0.45 ± 0.08	0.40 ± 0.08	0.39 ± 0.10	0.01 ± 0.01	0.01 ± 0.01
IV: 300–400 m	d	0.52 ± 0.08	0.47 ± 0.08	0.47 ± 0.10	0.01 ± 0.01	0.01 ± 0.02
V: >400 m	d	0.51 ± 0.05	0.45 ± 0.05	0.46 ± 0.05	0.01 ± 0.00	0.01 ± 0.01

<sup>a</sup> Satellite data recorded at solar elevation,  $\alpha_s = 26.8^\circ$ .

<sup>b</sup> Sample size for zone I is  $n_I = 253$ ,  $n_{II} = 1968$ ,  $n_{III} = 2938$ ,  $n_{IV} = 1829$  and  $n_V = 890$ .

<sup>c</sup> Standard deviation.

<sup>d</sup> Data saturation occurred.

Table 4. Satellite-derived surface albedo for five height zones on Austre Brøggerbreen recorded on 31 August 1988<sup>a</sup>.

Height zone <sup>b</sup>	TM Band					
	1	2	3	4	5	7
I: 50–100 m	0.20 ± 0.02 <sup>c</sup>	0.24 ± 0.02	0.21 ± 0.02	0.21 ± 0.02	0.02 ± 0.00	0.01 ± 0.00
II: 100–200 m	0.28 ± 0.03	0.31 ± 0.03	0.28 ± 0.03	0.31 ± 0.04	0.03 ± 0.01	0.02 ± 0.01
III: 200–300 m	0.36 ± 0.04	0.42 ± 0.04	0.38 ± 0.05	0.43 ± 0.06	0.06 ± 0.04	0.05 ± 0.03
IV: 300–400 m	0.45 ± 0.05	0.52 ± 0.06	0.48 ± 0.07	0.54 ± 0.09	0.09 ± 0.04	0.08 ± 0.04
V: >400 m	0.44 ± 0.03	0.49 ± 0.04	0.43 ± 0.04	0.50 ± 0.06	0.08 ± 0.01	0.05 ± 0.01

<sup>a</sup> Satellite data recorded at solar elevation,  $\alpha_s = 18.6^\circ$ .

<sup>b</sup> Sample size for zone I is  $n_I = 246$ ,  $n_{II} = 1497$ ,  $n_{III} = 2695$ ,  $n_{IV} = 1366$  and  $n_V = 736$ .

<sup>c</sup> Standard deviation.

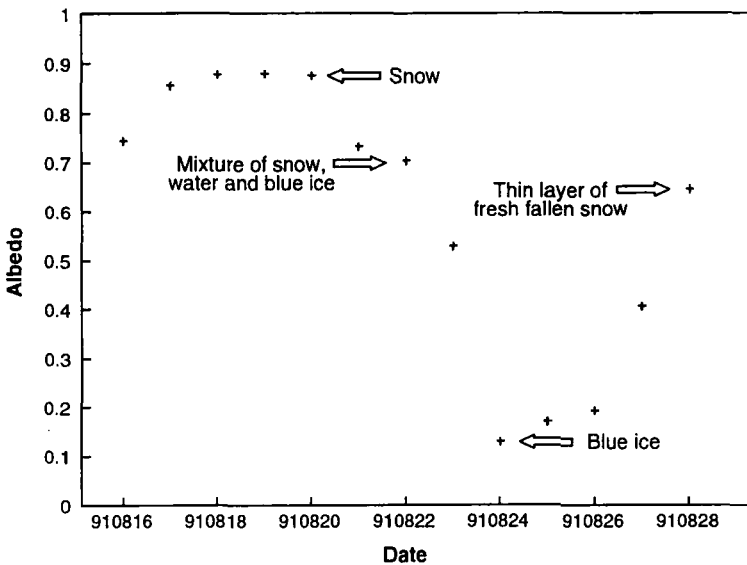


Fig. 9. Daily mean albedo of Austre Brøggerbreen at an elevation of 300 m a.s.l. The data clearly demonstrates how the reflectance decreases as the surface character turns from snow to blue ice from 16–24 August. At the end of the period, fresh snow started to accumulate on the blue ice surface. In situ measurements were recorded by a Kipp and Zonen CM 7 albedometer with an effective wave length range of 300 to approximately 2500 nm.

Table 5. Satellite-derived surface albedo for five height zones on Midre Lovénbreen recorded on 7 August 1987<sup>a</sup>.

Height zone <sup>b</sup>	TM Band					
	1	2	3	4	5	7
I: 50–100 m	0.22 ± 0.03 <sup>c</sup>	0.21 ± 0.02	0.18 ± 0.02	0.14 ± 0.02	0.01 ± 0.00	0.01 ± 0.00
II: 100–200 m	0.26 ± 0.04	0.28 ± 0.05	0.23 ± 0.05	0.20 ± 0.06	0.01 ± 0.00	0.00 ± 0.00
III: 200–300 m	0.40 ± 0.06	0.45 ± 0.07	0.39 ± 0.07	0.38 ± 0.09	0.01 ± 0.00	0.01 ± 0.00
IV: 300–400 m	d	0.54 ± 0.05	0.47 ± 0.05	0.48 ± 0.06	0.01 ± 0.01	0.01 ± 0.01
V: >400 m	d	0.56 ± 0.06	0.51 ± 0.07	0.53 ± 0.08	0.01 ± 0.02	0.01 ± 0.01

<sup>a</sup> Satellite data recorded at solar elevation,  $\alpha_s = 26.8^\circ$ .

<sup>b</sup> Sample size for zone I is  $n_I = 378$ ,  $n_{II} = 844$ ,  $n_{III} = 1126$ ,  $n_{IV} = 958$  and  $n_V = 855$ .

<sup>c</sup> Standard deviation.

<sup>d</sup> Data saturation occurred.

Eaton 1975; Carroll & Fitch 1981; McGuffie & Henderson-Sellers 1985). Thus, the chance for an electromagnetic wave to escape from the snow pack without being absorbed is improved by low incident angles. This effect on the albedo is symmetric around local noon. The solar elevation was

$34.0^\circ$  at 13:30 and  $31.6^\circ$  at 15:30 (both local summer time) at the measuring site on 9 June. Considering the small reduction in solar elevation, a significant increase in albedo due to a lowered solar angle is not likely (Wiscombe & Warren 1980). Concerning the second con-

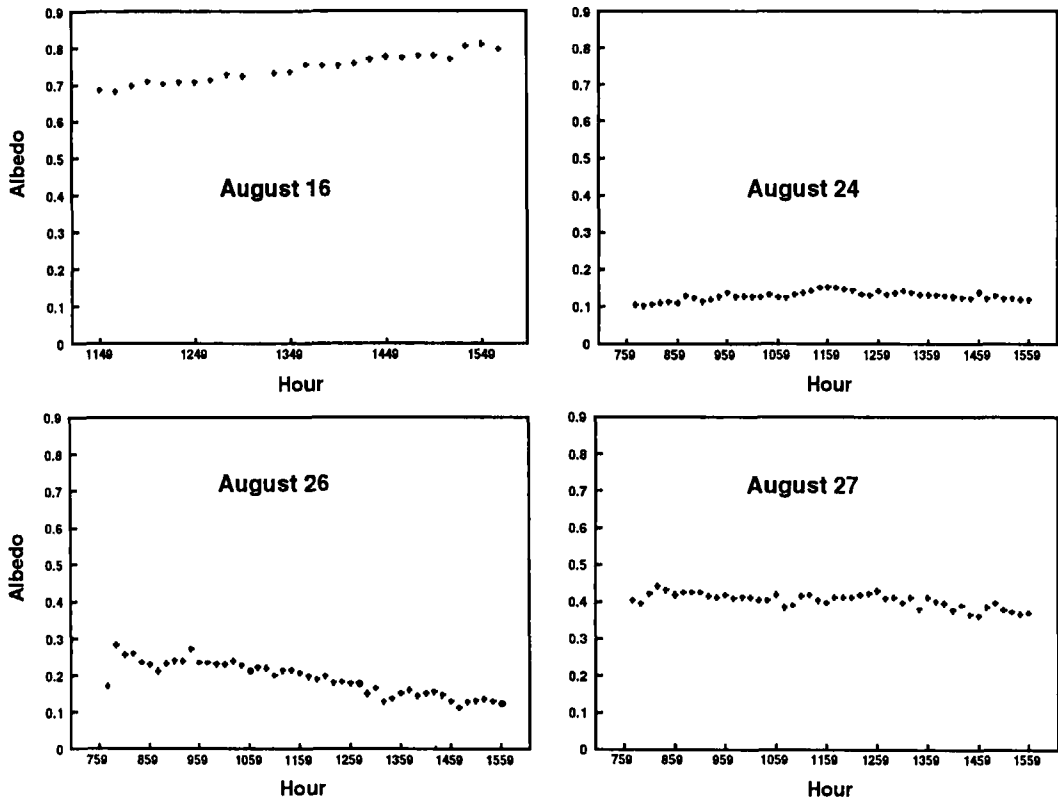


Fig. 10. In situ albedo measurements from Austre Brøggerbreen (300 m.a.s.l.) on 16, 24, 26 and 27 August 1991. The logging interval is 10 min.

Table 6. Satellite-derived surface albedo for five height zones on Midre Lovénbreen recorded on 31 August 1988<sup>a</sup>.

Height zone <sup>b</sup>	TM Band					
	1	2	3	4	5	7
I: 50–100 m	0.20 ± 0.03 <sup>c</sup>	0.22 ± 0.03	0.19 ± 0.02	0.19 ± 0.03	0.02 ± 0.00	0.01 ± 0.00
II: 100–200 m	0.28 ± 0.03	0.30 ± 0.04	0.26 ± 0.04	0.28 ± 0.04	0.04 ± 0.01	0.03 ± 0.01
III: 200–300 m	0.38 ± 0.03	0.41 ± 0.03	0.36 ± 0.03	0.41 ± 0.05	0.06 ± 0.01	0.05 ± 0.01
IV: 300–400 m	0.47 ± 0.05	0.51 ± 0.06	0.47 ± 0.07	0.54 ± 0.09	0.09 ± 0.02	0.07 ± 0.02
V: >400 m	0.51 ± 0.06	0.59 ± 0.07	0.54 ± 0.07	0.65 ± 0.10	0.10 ± 0.03	0.08 ± 0.02

<sup>a</sup> Satellite data recorded at solar elevation,  $\alpha_s = 18.6^\circ$ .

<sup>b</sup> Sample size for zone I is  $n_I = 473$ ,  $n_{II} = 762$ ,  $n_{III} = 1057$ ,  $n_{IV} = 895$  and  $n_V = 463$ .

<sup>c</sup> Standard deviation.

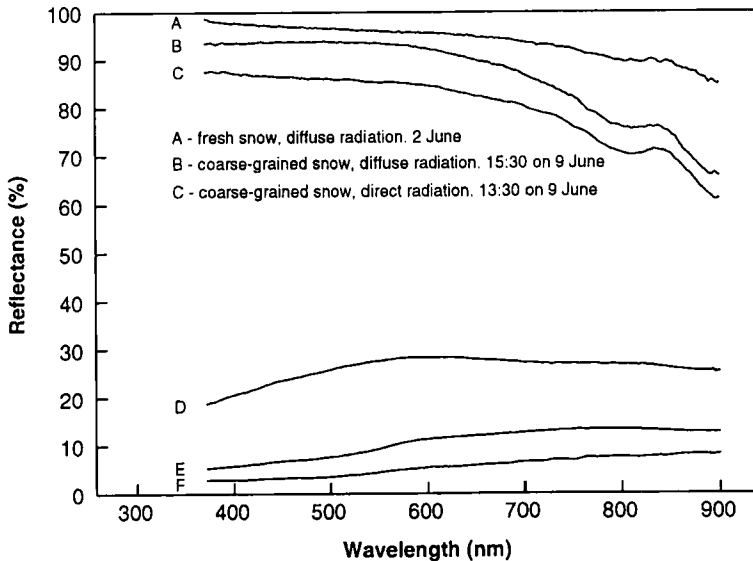


Fig. 11. Reflectance curves for (A) fresh snow on 2 June, 1992 (overcast), (B) coarse-grained snow at 15:30 local summer time on 9 June 1992 (overcast), (C) coarse-grained snow at 13:30 local summer time on 9 June (clear sky), (D), (E) and (F) moraines at the terminus of Austre Brøggerbreen on 10 June 1992. Note the increase in spectral albedo within a two-hour period on 9 June due to the change from clear sky to overcast weather conditions. All measurements were made at nadir viewing angles.

tribution (2), the metamorphism of the snow pack is an irreversible process and normally results in a decrease of the albedo. A crust layer due to night-time freezing was registered all the time on 9 June. Consequently, it seemed like the changes of snow surface characteristics due to metamorphism were small, at least during a period of only two hours. Further, in this case, the two effects counteract each other.

If effects from solar angle, metamorphism and the instrument are discounted, the increase in average albedo from 0.812 to 0.869 (i.e. 7 per cent) from 13:30 (Curve C) to 15:30 (Curve B)

can most probably be attributed to the change from direct (Curve C) to diffuse radiation (Curve B). This is because clouds absorb a higher portion of infra-red than visible radiation. Thus, a relatively high portion of the visible radiation reaches the ground under cloudy conditions. Because the visible snow albedo is very high (>90%) compared to the near-infra-red albedo (about 50%), an increase in surface albedo is to be expected when the weather turns from clear sky at 13:30 till complete overcast conditions at 15:30 (Wendler & Kelley 1988).

Curves D, E and F show spectral signatures for

Table 7. Classification of snow surface conditions on 2, 3, 8, 9 and 10 June 1992, in accordance with Colbeck et al. (1985). The table presents the grain size in mm (E), % liquid water content by volume ( $\Theta$ ), density in  $\text{g}/\text{cm}^3$  ( $\rho$ ) and temperature at a depth of 2.5 cm in  $^{\circ}\text{C}$  (T). In addition, snow hardness (R) and grain size (mm) for the upper 20 cm of the snow pack is given. R is determined by the hand test where objects of different areas (i.e. fist, finger(s), pencil, knife blade) are gently pushed into the snow. The scale range from very low, low, medium, high, very high to ice.

	2 June (15 m.a.s.l.)	3 June (15 m.a.s.l.)	8 June (175 m.a.s.l.)	9 June (15 m.a.s.l.)	10 June (75 m.a.s.l.)
E	<1	<1	0.5-2	2-3	1-5
$\Theta$	—	7.5	10.4	0.3	0.8
$\rho$	0.218	0.370	0.570	0.476	0.426
T	-1.4	+0.3	+0.1	-0.7	+0.1
R, E	0-4 cm: Very low, <1 4-12 cm: High, 1-2 12-13 cm: Ice 13-21 cm: Medium, 1-2	0-6 cm: Low, <1 6-7 cm: Very high (crust), 1-2 7-10 cm: High, 1-2 10-11 cm: Ice 11-20 cm: Medium, 0.5-1.5	0-11 cm: Low, 0.5-2.0 11-16 cm: Low, 1-3 16-17 cm: Ice 17-21 cm: Low, 1-3	0-9 cm: Very high (crust), 2-3 9-19 cm: Low, 1-2	0-9 cm: High, 1-5 9-20 cm: Medium, 1-3

three different types of moraine found in the terminus area of Austre Brøggerbreen on 10 June 1992. Curve D displays spectral characteristics of stones with lengths between 5 and 40 cm. The average albedo is 0.259. Curve E is from a 2-4 cm thick layer of wet sand/silt overlaying the glacier ice. Curve E has an average albedo of 0.104. Finally, Curve F represents an area of dry stones with lengths between 2 and 15 cm and has an average albedo of 0.055.

#### Bidirectional reflectance of snow

Fig. 12 shows the spectral reflectance of snow for viewing angles  $0^{\circ}$  (nadir),  $15^{\circ}$ ,  $30^{\circ}$ ,  $45^{\circ}$  and  $60^{\circ}$  for viewing directions facing the sun, and  $90^{\circ}$  and  $180^{\circ}$  away from the sun. The reflectance curves from 9 June were acquired with clear sky conditions. Reflectance values larger than 1.0 appear, especially for the largest viewing angles. Off-nadir reflectance values  $>1.0$  are reported to be quite common for dry snow (Hall et al. 1992b) and are also published by Dozier et al. (1988). This is because snow can reflect light specularly, and more light may be reflected than is incident upon the snow in one particular direction. Measurements facing the sun on 9 June (Fig. 12) display the largest anisotropy even though such anisotropy is seen in the scan sequences facing away from the sun as well. In fact, some specular reflection occur at all azimuth angles (Dirnhirn & Eaton 1975). On 9 June, the integrated albedo increases with 0.07 from nadir to  $15^{\circ}$  off-nadir in the viewing direction facing the sun while the increase is 0.04 from nadir to  $15^{\circ}$  off-nadir in the viewing direction facing  $90^{\circ}$  away from the sun. Similarly, the increase from nadir to  $45^{\circ}$  off-nadir is 0.20 and 0.06 for the two viewing directions. The reflectance curves taken  $180^{\circ}$  away from the sun on 9 June are affected by shadows from the tripod where the spectrometer was fastened (Fig. 12).

Similar reflectance characteristic curves are displayed for 8 June (Fig. 12). These curves were acquired during overcast weather and thus the incoming radiation was mainly diffuse. Even during overcast weather with diffuse incoming radiation, the radiation scatters mostly in the forward direction (Kanestrøm 1975). The effective solar elevation for overcast weather conditions (i.e. diffuse radiation) is normally estimated to be  $40^{\circ}$  (Warren 1982). The integrated albedo increases 0.11, 0.10 and 0.11 from nadir to  $15^{\circ}$  off-nadir for

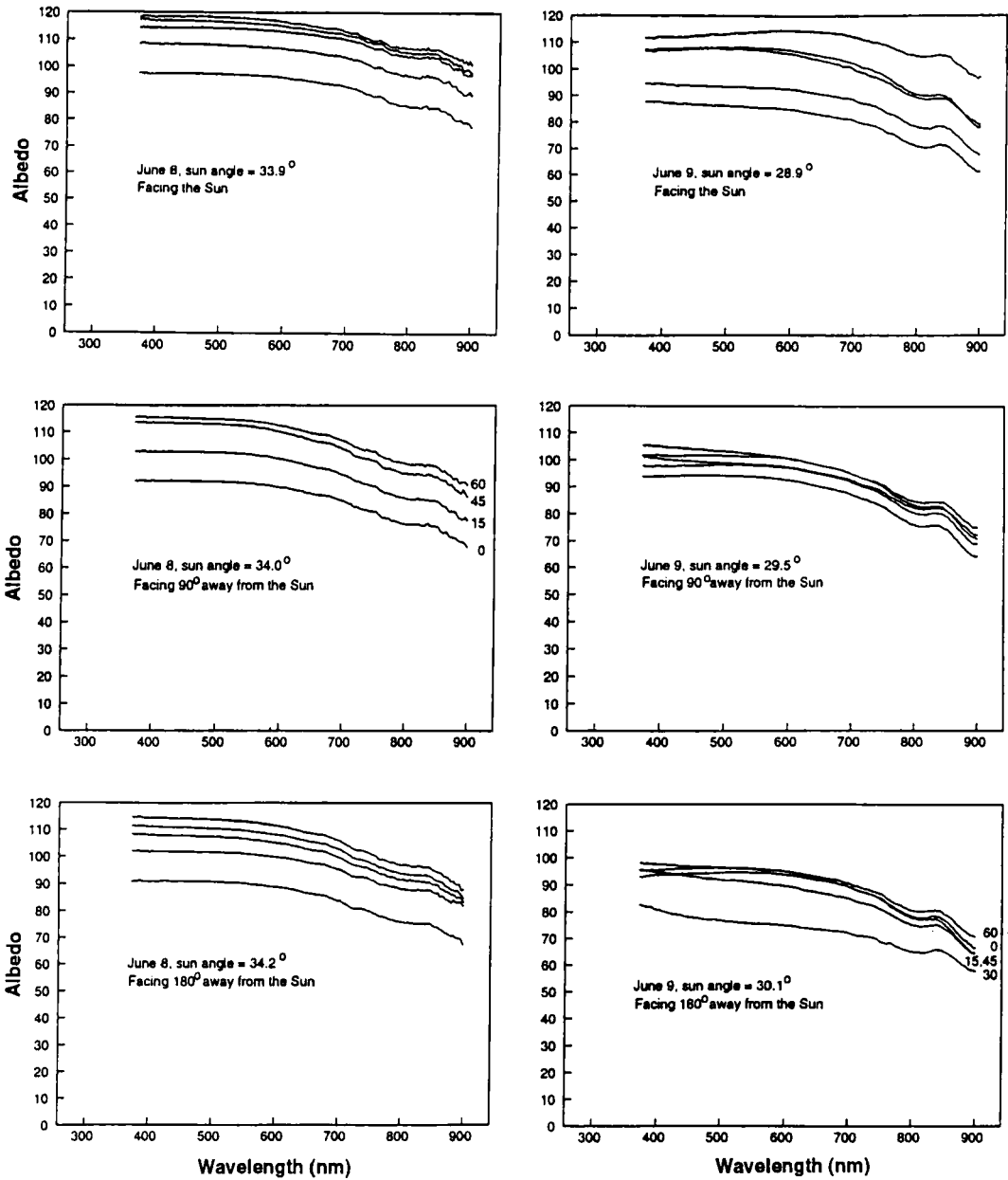


Fig. 12. Reflectance curves of snow measured at viewing angles 0° (nadir), 15°, 30°, 45° and 60° for viewing directions facing the sun, and 90° and 180° away from the sun, on 8 June and 9 June 1992. Measurements from 8 June were taken on Austre Brøggerbreen at 175 m.a.s.l. in overcast weather while the reflectance curves from 9 June were obtained during clear sky conditions on a snow-covered site downstream from the terminus of Austre Brøggerbreen (15 m.a.s.l.).

the viewing direction facing the sun, 90° and 180° away from the sun, respectively. Similarly, the increase in albedo is 0.20, 0.20 and 0.19 from nadir to 45° off-nadir. However, because of the overcast weather, this represents a situation

where Landsat TM images are useless for studies of surface characteristics.

Fig. 13 displays the spectral reflectance of snow from 2–3, 8 and 10 June. On 2 June and 3 June, the surface consists of freshly fallen snow with

characteristic grain size less than 1 mm (Table 7). The snow on 8 June and 10 June was considerably more metamorphosed with larger snow grains (Table 7). This change in snow grain size should have little effect on the visible albedo but a larger effect on the near-infra-red albedo (Wiscombe & Warren 1980; Warren 1982). In accordance with the theory, the curves have a similar slope in the visible region while the drop in the near-infra-red albedo is more pronounced on 8 June and 10 June than on 2 June and 3 June (Fig. 13). A possible source of error is that the measurements from 2 June and 3 June are facing  $180^\circ$  away from the sun while the curves from 8 June and 10 June are facing towards the sun. However, the measurements presented in Fig. 12 demonstrate that a change in azimuth viewing direction mainly leads to a parallel displacement and not an alteration

of the shape and slope of the reflectance curves. This is also seen in the work reported by Dozier et al. (1988) It thus seems likely that the drop in the near-infrared albedo on 8 June and 10 June is caused by an increase in snow grain size (Fig. 13).

Table 8 presents the integrated albedo for all the curves shown in Figs. 12 and 13. The increase of albedo (in per cent) due to the bidirectional reflectance of snow is 8, 15, 19 and 26 per cent when the viewing angles are  $15^\circ$ ,  $30^\circ$ ,  $45^\circ$  and  $60^\circ$ , respectively. In studies where satellite images are used for *absolute* calculations of surface reflectance, the specular reflection of snow crystals must be accounted for. However, the specular properties of the snow can vary considerably during a short time and it may be difficult to estimate the effect of bidirectional reflectance at a given

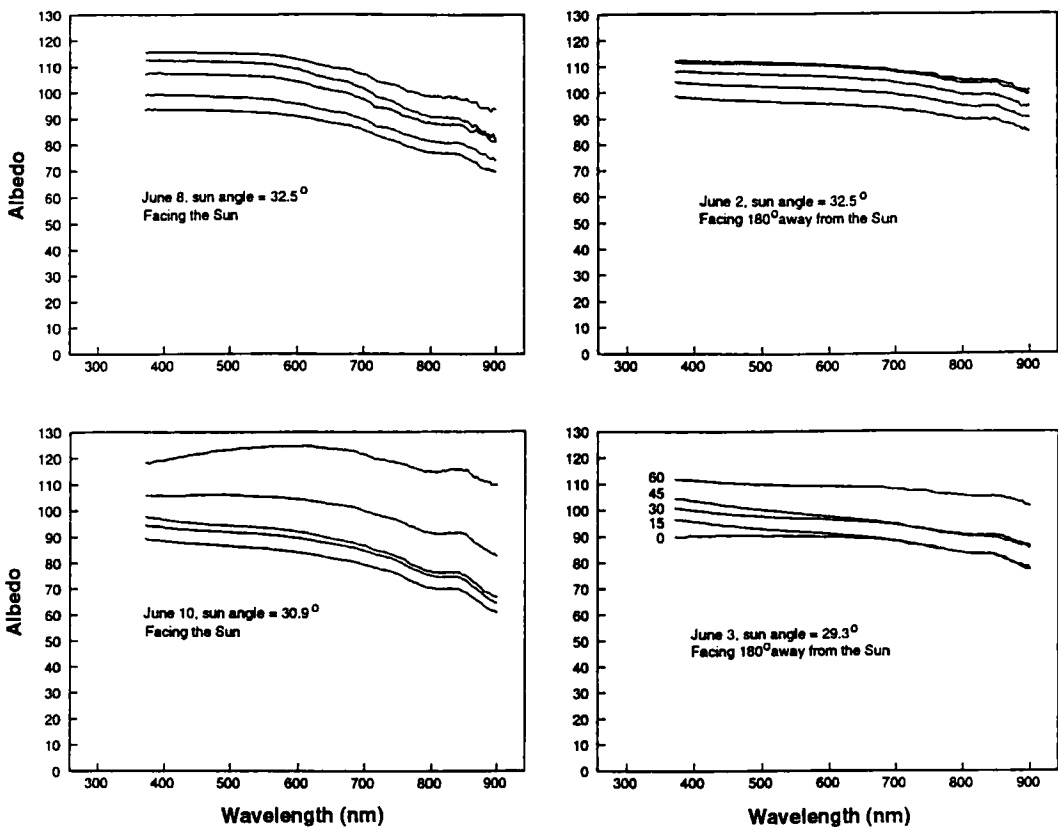


Fig. 13. Spectral reflectance of snow from 2, 3, 8 and 10 June. On 2 June and 3 June the surface consisted of fresh fallen snow with grain sizes less than 1 mm. The snow on 8 June and 10 June was considerably more metamorphosed with a characteristic snow grain size of 1–5 mm. The decrease in the near-infra-red albedo is more pronounced in the curves taken on 8 June and 10 June, reflecting the effect of snow grain size on the spectral albedo.

**Table 8.** The table presents the integrated albedo of snow from measurements taken on 2, 3, 8, 9 and 10 June (Figs. 12 and 13). The increase (in percent) relative to the albedo at nadir due to bidirectional reflectance of snow is given for viewing angles 15°, 30°, 45° and 60° off-nadir for (1) all measurements, (2) measurements facing the sun (clear sky) and (3) measurements facing 90° away from the sun (clear sky). The measurements include snow in various degrees of metamorphosis.

	Nadir	15°	30°	45°	60°
Albedo, all measurements	86.65	93.84	99.65	103.24	109.09
Increase of albedo (%)		8.30	15.01	19.15	25.90
Albedo, facing the sun, clear sky	80.22	86.46	94.32	100.25	115.27
Increase of albedo (%)		7.79	17.58	24.98	43.70
Albedo, 90° away from the sun, clear sky	87.22	91.57	94.76	92.88	96.18
Increase of albedo (%)		4.99	8.64	6.49	10.27

point of time without reference ground truth measurements.

## Conclusions

The study uses both satellite-derived and in situ measurements to indicate the large range of surface reflectance which may be present on a glacier, especially at the end of the mass balance year. The variations in glacier albedo are shown to be large in several respects: (1) from one year to another, (2) at different areas of the glacier at one point of time and (3) on one fixed location during a period of a few days. The albedo affects the energy absorption of the glacier and thus its mass balance as well as the Earth-atmosphere energy balance. Consequently, the monitoring of glacier reflectance is important for local, regional and global energy exchange calculations.

The near-infra-red snow albedo is sensitive to changes in characteristic snow grain size. Spectral measurements show a distinct drop in the near-infra-red albedo as the snow metamorphoses, i.e. the grain size increases. The visible albedo is little affected by the variation of grain size. Clouds affect the snow albedo by introducing a spectral shift to the incoming radiation. It is shown that the integrated snow albedo (370–900 nm) increases by 7% due to the change from clear sky to overcast weather. With respect to climate change, there are concerns that changes in the cloud conditions such as type, height and distribution may occur if the climate changes. As seen above, an increased amount of cloud coverage can in isolation give a negative feedback on the snow surface (shortwave) energy exchange system by increasing the snow albedo.

Metamorphosed snow is an anisotropic reflec-

tor and reflects light specularly. Thus, more light may be reflected than is incident upon the snow in one particular direction. The increases in albedo relative to the nadir albedo for the viewing angles 15°, 30°, 45° and 60° for measurements facing the sun (clear sky) were calculated to be 8, 18, 25 and 44%, respectively (Table 8). Similarly, for all measured directions, the increase in albedo was computed to be 8, 15, 19 and 26%. Consequently, Landsat TM derived snow reflectance for metamorphosed snow in rugged terrain cannot be considered *absolute* albedo values. A Digital Terrain Model of a study area is needed to correct for the effects introduced by the topography and the anisotropic snow reflectance. Finally, the effect of anisotropic snow reflectance varies with the state of the snow and must be updated to obtain accurate corrections at a given point of time. This can be done by reference ground truth measurements, for example.

*Acknowledgements.* – The author would like to thank O. Løvøll, A. Løvøll and O. Bruland at the Norwegian Institute of Technology and K. Sand at the SINTEF Norwegian Hydrotechnical Laboratory for valuable assistance during the field work in 1991 and 1992. Further, acknowledgements are addressed to J. O. Hagen at the Norwegian Polar Institute for providing essential data and J. Maedel at the University of British Columbia for substantial help and guidance during the processing of the satellite data. The Norwegian National Committee for Hydrology is acknowledged for their financial support.

## References

- Benson, C. S. 1959: Physical investigations on the snow and firn of northwest Greenland: 1952, 1953 and 1954. *SIPRE Res. Rep.* 26.
- Benson, C. S. 1967: Polar regions snow cover. Pp. 1039–1063 in Oura, H. (ed.): *Physics of snow and ice. International Conference of Low Temperature Science 1966 Proceedings. Vol. 1. Part 2.* Sapporo, Hokkaido University.

- Benson, C. S. & Motyka, R. J. 1979: Glacier-volcano interactions on Mt. Wrangell, Alaska. University of Alaska, Fairbanks. Geophysical Institute. Annual Report 1977-78. pp. 1-25.
- Bryazgin, N. N. & Koptev, A. P. 1969: O spektral'nom al'bedo snezhnoledyanogo pokrova (Spectral albedo of a snow ice cover). *Problemy Arktiki i Antarktiki* 31, 79-83.
- Carroll, J. J. & Fitch, B. W. 1981: Dependence of snow albedo on solar elevation and cloudiness at the South Pole. *J. Geophys. Res.* 86, 5271-5276.
- Choudhury, B. J. & Chang, A. T. C. 1979: Two-stream theory of reflectance of snow. *IEEE Trans. Geosci. and Remote Sensing* 17, 63-68.
- Colbeck, S., Akitaya, E., Armstrong, R., Gubler, H., Lafcuille, J., Lied, K., McClung, D. & Morris, E. 1985: *The international classification for seasonal snow on the ground*. Issued by the International Commission on snow and ice of the International Association of Scientific Hydrology; co-issued by the International Glaciological Society. 23 pp.
- Dirmhirn, I. & Eaton, F. O. 1975: Some characteristics of the albedo of snow. *J. Appl. Meteorol.* 14, 375-379.
- Dozier, J. 1984: Snow reflectance from Landsat-4 thematic mapper. *IEEE Trans. Geosci. and Remote Sensing* Ge-22, 323-328.
- Dozier, J. 1985: Spectral signature of snow in visible and near-infrared wavelengths. *Proc. 3rd Internat. Colloq. Spectral Signatures of Objects in Remote Sensing, Paris, ESA SP-247*, 437-442.
- Dozier, J. 1989: Spectral signature of alpine snow cover from the Landsat thematic mapper. *Remote Sensing Environ.* 28, 9-22.
- Dozier, J., Schneider, S. R. & McGinnis, D. F. 1981: Effect of grain size and snowpack water equivalence on visible and near-infrared satellite observations of snow. *Water Resources Res.* 17, 1213-1221.
- Dozier, J., Davis, R. E., Chang, A. T. C. & Brown K. 1988: The spectral bidirectional reflectance of snow. *Proc. 4th Internat. Colloq. Spectral Signatures of Objects in Remote Sensing, France, ESA SP-287*, 87-92.
- Hagen, J. O. & Liestøl, O. 1990: Long-term glacier mass balance investigations in Svalbard, 1950-88. *Ann. Glaciol.* 14, 102-106.
- Hagen, J. O., Korsen, O. M. & Vatne, G. 1991: Drainage pattern in a subpolar glacier: Brøggerbreen, Svalbard. *Norwegian Natl. Comm. Hydrol. Rep.* 23, 121-131.
- Hall, D. K. & Ormsby, J. P. 1983: Use of SEASAT synthetic aperture radar and LANDSAT multispectral scanner subsystem data for Alaska glaciology studies. *J. Geophys. Res.* 88(C3), 1597-1607.
- Hall, D. K., Ormsby, J. P., Bindschadler, R. A. & Siddalingaiah, H. 1987: Characterization of snow and ice reflectance zones on glaciers using Landsat thematic mapper data. *Ann. Glaciol.* 9, 104-108.
- Hall, D. K., Chang, A. T. C. & Siddalingaiah, H. 1988: Reflectances of glaciers as calculated using Landsat-5 thematic mapper data. *Remote Sensing Environ.* 25, 311-321.
- Hall, D. K., Chang, A. T. C., Foster, J. L., Benson, C. S. & Kovalick, W. M. 1989: Comparison of in situ and Landsat derived reflectance of Alaskan glaciers. *Remote Sensing Environ.* 28, 23-31.
- Hall, D. K., Bindschadler, R. A., Foster, J. L., Chang, A. T. C. & Siddalingaiah, H. 1990: Comparison of in situ and satellite-derived reflectances of Forbindels Glacier, Greenland. *Int. J. Remote Sensing* 11(3), 493-504.
- Hall, D. K., Williams, R. S. & Bayr, K. J. 1992a: Glacier recession in Iceland and Austria. *Eos Trans. Am. Geophys. Union* 73(12), 129, 135, 141.
- Hall, D. K., Foster, J. L. & Chang, A. T. C. 1992b: Reflectance of snow as measured in situ and from space in sub-arctic areas in Canada and Alaska. *IEEE Trans. Geosci. and Remote Sensing* 30(3), 634-637.
- Holben, B. N. & Justice, C. O. 1979: Evaluation and modeling of the topographic effect on the spectral response from nadir pointing sensors. NASA TM 80305, Goddard Space Flight Center, Greenbelt, Maryland.
- Kanestrøm, I. 1975: Stråling i atmosfæren (Radiation in the Atmosphere). Report. Geophysical Institute, University of Oslo, 204 pp.
- Liestøl, O. 1977: Pingos, springs and permafrost in Spitsbergen. *Norsk Polarinst. Årbok* 1975, 7-29.
- Lillesand, T. M. & Kiefer, R. 1987: *Remote sensing and image interpretation*. 2nd ed. John Wiley & Sons, New York. 721 pp.
- Markham, B. L. & Barker, J. L. 1986: Landsat MSS and TM post-calibration dynamic ranges, exoatmospheric reflectances and at-satellite temperatures. *EOSAT Technical Notes* 1, 3-8.
- McGuffie, K. & Henderson-Sellers, A. 1985: The diurnal hysteresis of snow albedo. *J. Glaciol.* 31(108), 188-189.
- Müller, F. 1962: Zonation in the accumulation area of the glaciers of Axel Heiberg Island, N.W.T., Canada. *J. Glaciol.* 4(33), 302-311.
- Orheim, O. & Lucchitta, B. K. 1988: Numerical analysis of Landsat thematic mapper images of Antarctica: Surface temperatures and physical properties. *Ann. Glaciol.* 11, 109-120.
- Parrot, J. F., Lyberis, N., Lefauconnier, B. & Manby, G. 1993: SPOT multispectral data and digital terrain model for the analysis of ice-snow fields on arctic glaciers. *Int. J. Remote Sensing* 14(3), 425-440.
- Paterson, W. S. B. 1981: *The physics of glaciers*. 2nd ed. Pergamon Press, New York. 380 pp.
- Proy, C., Tanré, D. & Deschamps, P. Y. 1989: Evaluation of topographic effects in remotely sensed data. *Remote Sensing Environ.* 30, 21-32.
- Sand, K. Berntsen, E., Hagen, J. O. & Repp, K. 1991: Climate related research in Svalbard. *Norwegian Nat. Comm. Hydrol. Rep.* 23, 203-217.
- Schytt, V. 1981: The net balance of Storglaciären, Kebnekaise, Sweden, related to the height of the equilibrium line and to the height of the 500 mb surface. *Geogr. Ann.* 63A(3-4), 213-223.
- Steffen, K. 1987: Bidirectional reflectances of snow, in large scale effects of seasonal snow cover. Pp. 415-425 in Goodison, B. E., Barry, R. G. & Dozier, J. (eds.): *Proceedings of the IAHS Symposium, Canada*.
- Tanré, D., Deroo, C., Duhaut, P., Herman, M., Morcrette, J. J., Perbos, J. & Deschamps, P. Y. 1990: Description of a computer code to simulate the satellite signal in the solar spectrum: the 5S code. *Int. J. Remote Sensing* 11, 659-668.
- Wakahama, G., Kuroiwa, D., Hasemi, T. & Benson, C. S. 1976: Field observations and experimental and theoretical studies on the superimposed ice of McCall Glacier, Alaska. *J. Glaciol.* 16(74), 135-149.
- Warren, S. G. 1982: Optical properties of snow. *Rev. Geophys. Space Phys.* 20(1), 67-89.
- Warren, S. G. & Wiscombe, W. J. 1985: Dirty snow after nuclear war. *Nature* 313, 467-470.
- Wendler, G. & Kelley, J. 1988: On the albedo of snow in

- Antarctica: A contribution to I.A.G.O. *J. Glaciol.* 34, 19–25.
- Williams, R. S., Hall, D. K. & Benson, C. S. 1991: Analysis of glacier facies using satellite techniques. *J. Glaciol.* 37(125), 120–128.
- Wiscombe, W. J. & Warren, S. G. 1980: A model for the spectral albedo of snow. I: Pure snow. *J. Atmos. Sci.* 37, 2712–2733.
- Young, G. J. 1981: The mass balance of Peyto Glacier, Alberta, Canada, 1965 to 1978. *Arct. Alp. Res.* 13(3), 307–318.
- Zeng, Q., Cao, M., Feng, X., Liang, F., Chen, X. & Sheng, W. 1984: A study of spectral reflection characteristics for snow, ice and water in the north of China. *Hydrological Applications of Remote Sensing and Remote Data Transmission. Proceedings of the Hamburg Symposium. IAHS Publication No. 145*, 451–462.
- Østrem, G. 1975: ERTS data in glaciology: An effort to monitor glacier mass balance from satellite imagery. *J. Glaciol.* 15(73), 403–415.